

METHOD FOR ASSESSING TRUE STRESS-STRAIN CURVES AFTER NECKING USING CYLINDRICAL TENSILE SPECIMENS: THEORETICAL BACKGROUND AND EXPERIMENTS¹

Grace Kelly Quarteiro Ganharuf²
Gustavo Henrique Bolognesi Donato³

Abstract

Simulations including severe plasticity have undergone significant expansion during the last years (e.g. fracture mechanics FE models including ductile tearing), which demand accurate true stress-strain data until fracture. However, the occurrence of plastic instability (necking) on tensile specimens complicates the direct assessment of σ - ε curves due to the imposition of a complex triaxial stress state. Previous results published by current authors demonstrated that even the widespread Bridgman's correction presents limitations, which motivated the proposal of a new model to describe the geometrical evolution of necking (in which the geometrical dimensionless parameter a/R is proportional to strain ε). In this context, this work presents two contributions: i) first, experiments regarding the geometrical evolution of necking were largely extended incorporating 10 materials to corroborate the validity of the proposed model (including Carbon and stainless steels, and copper); ii) second, for the same materials, the necking region was investigated in more details to verify to which extent an osculating circle well describes the high deformation region; iii) finally, an adapted Bridgman's model was proposed, followed by recommended practices for tensile testing. The results provide further support to σ - ε assessment until final fracture considering severe plasticity and demanding less physical measurements.

Key words: Plastic instability; Bridgman correction; Tensile test; True stress-strain data.

¹ Technical contribution to 68th ABM International Congress, July, 30th to August 2nd, 2012, Belo Horizonte, MG, Brazil.

² Mechanical engineer. Master student, Mechanical Engineering Department, FEI, São Bernardo do Campo, Brazil; gracekellyq@yahoo.com.br

³ Mechanical engineer. D.Sc. Professor, Mechanical Engineering Department, FEI, São Bernardo do Campo, Brazil; gdonato@fei.edu.br.

1 INTRODUCTION

Numerical elastic-plastic simulations including severe plasticity have undergone significant expansion during the last decades in order to better describe physical large strain phenomena (e.g. refined fracture mechanics finite element models including ductile tearing or generalized yielding).^(1,2) In addition, the most accurate levels for structural integrity evaluation of structures containing cracks based on recommended practices such as API-579⁽³⁾ and BS 7910⁽⁴⁾ can only be applied if nonlinear stress analyses can be conducted to describe stress fields and crack driving forces (J -integral or CTOD, for example). However, one limitation to increase the accuracy of such models is the reliable experimental characterization of true stress-strain curves from simple uniaxial tensile tests after necking (plastic instability), which complicates the direct assessment of the true stress-strain curves until failure.

Necking or localized deformation begins at the maximum load of a conventional tensile test, where the increase in stress due to the decrease in the cross-sectional area of the specimen becomes greater than the increase in the load-carrying capacity of the metal due to strain hardening.⁽⁵⁾ Considering cylindrical specimens made of isotropic materials (which is the case of this study), only one instability phenomenon takes place and necking results symmetric around the tensile axis (axisymmetric). Physically, the instability condition means that deformation proceeds without the need for extra load (P), which can be defined in the form $dP = 0$, where $P = \sigma A$. Applying the chain rule and assuming constant volume during plastic deformation, tensile instability takes place when $d\sigma/d\varepsilon = \sigma$,⁽⁶⁾ which means that the point of necking can be predicted from the true-stress (σ) – true-strain (ε) curve by finding the point where the rate of straining equals the applied stress.

Figure 1a illustrates a round tensile specimen after instability and defines all geometric features that describe the neck. Most theories assume that the neck can be fully characterized by an osculating circle (with radius R) combined to the minimum cross-section radius (a). In this work, some extra geometrical features are indicated for completeness and exploratory purposes (for example, the circular sector θ between the inflection points of the neck).

When plastic instability takes place, deformation tends to concentrate in one specific region as illustrated by Figure 1a. A closer look to the smallest cross-section (Figure 1b) reveals that adjacent material layers tend to contract in the transverse direction in a different manner. Consequently, the opposition to flow caused by the displacement mismatch of the surrounding material establishes a complex triaxial stress state in each layer, as presented for a generic volume by Figure 1b. The necked region thus acts as a mild notch, whose equilibrium produces radial (σ_r) and transverse (σ_t) stresses which “spuriously” raise the value of the longitudinal stress (σ_z) required to promote plastic flow.^(5,6) Therefore, these overestimated stresses must be deducted from the experimental stress-strain curves in order to support numerical simulations and guarantee similitude between real structures and small-scale specimens.⁽⁶⁻⁸⁾

Figure 1c presents a typical stress-strain curve for ductile metallic materials. Engineering stress (S) vs. engineering strain (e) curve (line between points A and C) can be easily obtained based on original specimen dimensions and experimental data as presented by Equation 1.⁽⁶⁾ Assuming volume maintenance and uniform transverse deformation along specimen’s length, Equation 2 allows respective true stress (σ) and true strain (ε) values to be directly computed (line between points A and D). However, Equation 2 is only valid until point D (which is based on data from

point B of the S - e curve), since this point represents the onset of necking ($dS/de = 0$; $dP = 0$) and thus the establishment of a triaxial stress state.

$$S = \frac{P}{A_0} ; e = \frac{\Delta L}{L_0} \tag{1}$$

$$\sigma = S(1 + e) ; \varepsilon = \ln(1 + e) \tag{2}$$

One alternative approach (Equation 3) to be able to compute true stresses and strains after necking is to compute stresses based on the instantaneous minimum cross-section area (A_{min}) of the specimen (which leads to σ_{net}) and strains based on the natural area reduction of the same section.^(5,6) This approach leads to the curve between points D and G of Figure 1c. Nevertheless, these stresses are higher than those required to cause flow if simple tension prevailed in the specimen, since σ_{net} incorporates the strain energy responsible for the aforementioned triaxial stress state. In this context, correction methods to discount triaxiality are of great academic and technological interest to provide accurate mechanical properties that guarantee similitude conditions and support to reliable numerical simulations. The curve between points D and F of Figure 1c illustrates such an approach providing a corrected equivalent stress-strain curve (being σ_c the corrected stress).

$$\sigma_{net} = \frac{P}{A_{min}} ; \varepsilon = \ln\left(\frac{A_0}{A}\right) \tag{3}$$

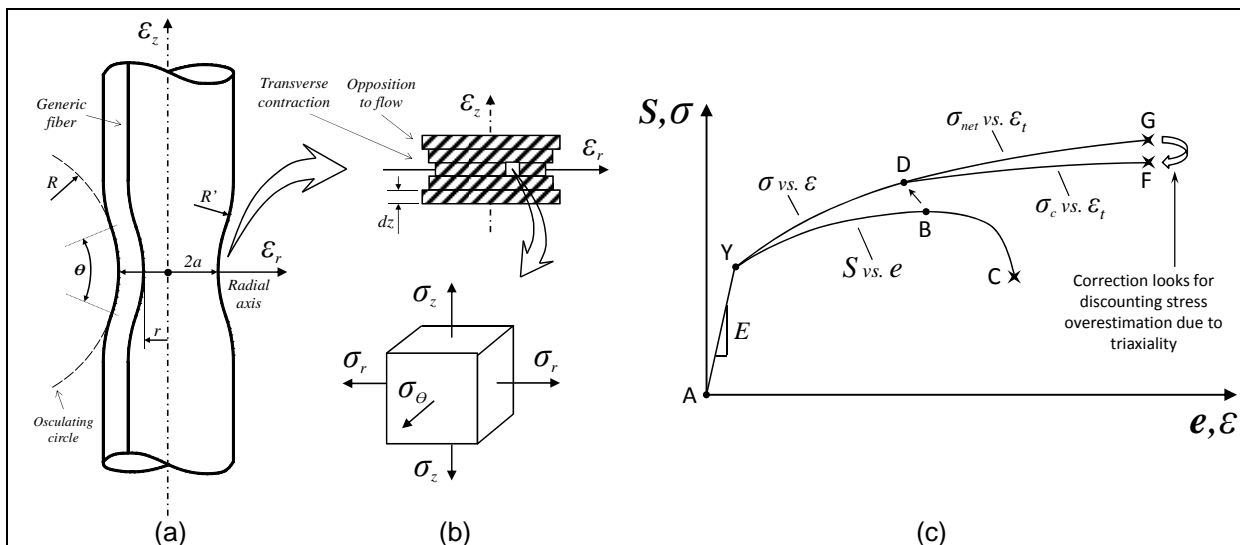


Figure 1. (a) Geometry of necking and (b) differential transverse contraction at the minimum cross-section providing a triaxial stress state. (c) Stress-strain curves considering engineering data (AYBC), true data before necking (AYD), true data not corrected (DG) and corrected for necking (DF).

2 METHODS FOR POST-NECKING σ - ε CORRECTION

Several methods have been proposed to correct stress-strain curves for triaxiality effects, some of them based on the classical theory of plasticity, while others rely upon common material constitutive models (e.g. Hollomon's equation) or iterative finite element computations.⁽⁹⁻¹¹⁾ The basis for all correction methods can be found in classical works from Bridgman, Davidenkov and Spiridonova⁽⁸⁾ and Thomason.⁽¹²⁾ A revision of those methods is presented in details in Ganharul, Azevedo e Donato.⁽¹⁾

Bridgman correction is considered the most accurate and theoretically supported and will be focused here.

2.1 The Bridgman Correction

The correction proposed by Bridgman⁽⁷⁾ is the most widespread methodology for correcting stress-strain curves for triaxiality effects. It is, however, only directly applicable to round specimens made of isotropic materials. Bridgman conducted a mathematical analysis based on equilibrium and material flow rules using the following assumptions:⁽⁵⁻⁷⁾

- the neck is approximated by the arc of an osculating circle with radius R (Figure 1). A similar curvature radius (ρ) can describe any general fiber drawn on the specimen parallel to its axis according to $(1/\rho)=(r/(aR))$;
- cross section of the neck remains circular after instability;
- σ_z , σ_r and σ_t are proportional principal stresses and von Mises criterion applies;
- strains are constant over the neck cross section. It means: assuming constant volume during plastic flow, $\varepsilon_r = \varepsilon_t = -\varepsilon_z/2$, supporting true strains (ε) from Equation 3.

The stress fields proposed by Bridgman to describe the neck must first satisfy equilibrium under large strain conditions (e.g. Equation 4 in z direction). In addition, using assumption 4, considering isotropic hardening and the boundary conditions provided by the free surface at the neck ($\sigma_z \neq 0$; $\sigma_r = \sigma_t = 0$), Bridgman proposed Equation 5 to describe the stress distributions at the minimum neck cross-section. One can realize that stresses for different radial positions (varying r) are only a function of geometrical parameters “ a ” and “ R ” from Figure 1. Figure 2 illustrates the stress fields predicted using these expressions and it can be realized that for $a/R = 0$ (absence of necking) the stress state is uniaxial, while for different neck geometries ($a/R \neq 0$) a triaxial stress state takes place. These fields thus allow, for the specimen centerline (largest stresses), the estimation of the equivalent (corrected) true stress (σ_c) based on σ_{net} and discounting triaxiality effects according to Equation 6.⁽⁷⁾ Curve DF from Figure 1c can thus be assessed using a correction factor (denoted here k) which can be applied to “net” stress-strain curves.

$$2\pi \int_0^a r \sigma_z dr = P \quad (4)$$

$$\sigma_r = \sigma_t = \frac{\sigma_{net}}{\left(1 + \frac{2R}{a}\right)} \left[\frac{\ln\left(\frac{a^2 + 2aR - r^2}{2aR}\right)}{\ln\left(1 + \frac{a}{2R}\right)} \right], \quad \sigma_z = \frac{\sigma_{net}}{\left(1 + \frac{2R}{a}\right)} \left[\frac{1 + \ln\left(\frac{a^2 + 2aR - r^2}{2aR}\right)}{\ln\left(1 + \frac{a}{2R}\right)} \right] \quad (5)$$

$$\sigma_c = \sigma_{net} [k] = \sigma_{net} \left[\frac{1}{\left(1 + 2\frac{R}{a}\right) \ln\left(1 + \frac{1}{2} \frac{a}{R}\right)} \right] \quad (6)$$

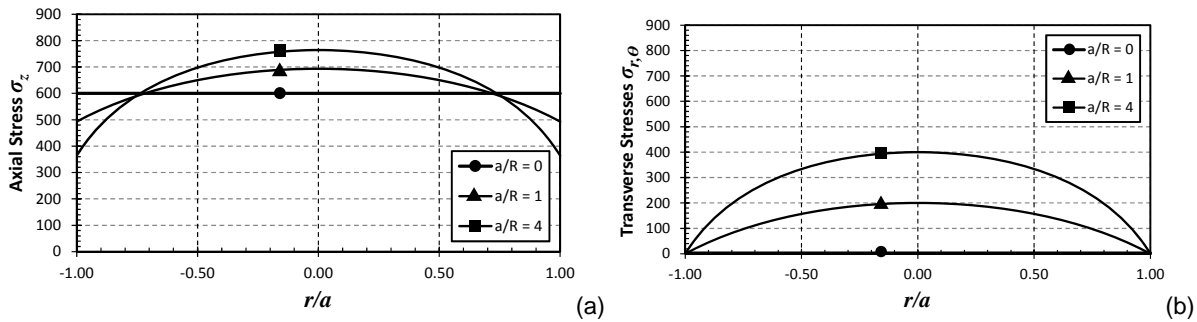


Figure 2. (a) σ_z and (b) $\sigma_{r,t}$ fields at minimum cross-section as a function of neck normalized radius (r/a) for different normalized neck evolution (a/R). Applied $\sigma_z = 600$ MPa.

Stress fields (Equation 5) and aforementioned assumption 4 (uniform strains at the neck) proposed by Bridgman were recently validated with very good agreement by Zhang and Li⁽¹³⁾ using FE models for strains up to ~ 0.50 – 0.60 . They also demonstrated that neck geometry describes the arc of a circle for steels (assumption 1). Consequently, it is reasonable to adopt Bridgman's fields as a reference here.

To avoid the need for real-time measurements of the neck during tests to apply Equation 6, Bridgman tested a series of materials (including Steels, Brass and Bronze)⁽⁷⁾ and found an interesting trend presented by Figure 3 for neck geometry as a function of true strain. Using a least squares procedure, he could find a relationship between a/R and ϵ and thus proposed a simplified k solution as presented by Equation 7. Consequently, a simplified Bridgman correction can be applied based only on real-time ϵ results (note that R parameter is not necessary for Equation 7, only a). This is of great technological relevance, since measuring the instantaneous minimum radius (despite not easy) is much easier than measuring the radius of the osculating circle (R) during the whole test. However, Equation 7 presents limitations and provides large errors as discussed next and in Ganharul⁽¹⁴⁾ by current authors. Bridgman admitted that all materials could be described by Equation 7 and it was proved by current authors not to be realistic, motivating this research effort.

$$k = 0.0684 [\log(\epsilon)]^3 + 0.0461 [\log(\epsilon)]^2 - 0.205 [\log(\epsilon)] + 0.825 \quad (7)$$

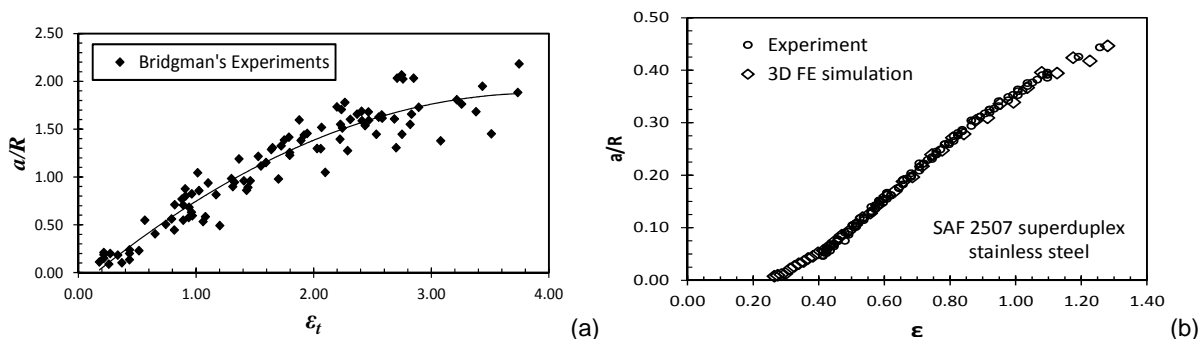


Figure 3. (a) Results obtained by Bridgman for the neck evolution as a function of ϵ for steels, brass and bronze.⁽⁷⁾ Markers for different materials were not identified by the author. (b) Results obtained by current authors⁽¹⁵⁾ for the neck evolution as a function of ϵ for a SAF 2507 superduplex stainless steel.

2.2 Adapted Bridgman Model Including Normalized Neck Geometry

In Figure 3a Bridgman did not identify different materials using different markers and results also revealed a large scatter for a/R (probably a result of the metrology apparatus available at that time). Recent studies conducted by current authors^(1,14,15) provided some extra results and made feasible some enhancements to Bridgman's original ideas as presented next. Figure 3b presents the a/R vs. ε evolution obtained by the authors for a specimen made of SAF 2507 superduplex stainless steel.⁽¹⁵⁾ All measurements for a/R and ε were performed using high resolution image analysis (which will be detailed next). First, the experimental results reveal almost no scatter; second, the a/R vs. ε evolution seems to be reasonably linear until final fracture; third, this evolution could be validated with very good agreement using refined nonlinear FE computations (details can be found in Azevedo e Donato⁽¹⁵⁾ and cannot be detailed here).

The results presented by Figure 3b, when considered together to the results presented in 2012 by current authors⁽¹⁾ motivated the proposal of a linear model for a/R vs. ε evolution in the form

$$\frac{a}{R} = \lambda \varepsilon + C, \quad (8)$$

where λ and C can be obtained from a linear fit to the data in Figure 3b. However, a limitation emerged during preliminary tests: different specimens presented the same slope λ but non-coincident parallel a/R vs. ε evolutions (different C). This is because the exact strain level for plastic instability can be influenced by the geometry of the specimens, misalignments, defects, among other details. A phenomenological discussion of necking phenomenon can solve this problem: the onset of necking is characterized by the last moment of uniform cross-sections, which leads to $R = \infty$ and thus $a/R = 0$. Recalling Equation 8, it means that ε for $a/R = 0$ represents the true strain for necking (denoted here ε_{neck}). This true strain for necking can be discounted from all data and only strains in the triaxial stress state considered (denoted $\varepsilon_{tri} = \varepsilon - \varepsilon_{neck}$). This approach leads to coincident trajectories and the proposed model becomes

$$\frac{a}{R} = \psi \varepsilon_{tri} = \psi (\varepsilon - \varepsilon_{neck}) \quad (9)$$

The model presented by Equation 9, when implemented in original Bridgman's equation (Equation 6) leads to an adapted correction in the form

$$\sigma_c' = \sigma_{net} [k'] = \sigma_{net} \left[\frac{1}{\left(1 + \frac{2}{\psi \varepsilon_{tri}}\right) \ln \left(1 + \frac{1}{2} \psi \varepsilon_{tri}\right)} \right] \quad (10)$$

The main objective of this investigation is to provide further support to the validity of Equation 9 and to the use of the proposed model of Equation 10, which demands less real-time physical measurements.

2.3 Experimental Program

Selected materials were tested under tension, including AISI 1010, 1020, 4140, ASTM A36, A285 and A516 Gr. 70 steels, AISI 304, 301 and SAF 2507 superduplex stainless steels and electrolytic copper. All tests were conducted based on ASTM E8/E8M standard⁽¹⁶⁾ and employed round conventional specimens. An MTS 810 testing machine (250 kN capacity) was employed under clip-gage displacement control (original gage length = 50 mm) to guarantee the desired 0.8 mm/min speed during the tests. Data acquisition rate was 30 Hz and all data were post-processed using MatLab routines to obtain mechanical properties and calibrate parameters.

2.4 High-definition Images Acquisition and Analysis

Looking for accuracy on the geometrical evolution of necking, real-time high-definition images were acquired during all tests using a Nikon D40 professional camera (15 megapixels) synchronized to the MTS machine. The main reason was to avoid the need for test interruption or mechanical measurements during necking phenomenon and the calibration process. Images were automatically captured based on a strain interval of 0.05% during the elastic regime, 0.10% during uniform plastic deformation and 0.05% after necking until failure.

An special image analysis algorithm was developed using MatLab platform and geometrical features presented by Figure 1 (a , R , θ , R' , among many others) could be obtained for each analyzed frame. Pixels calibration was based on original specimen's diameter, quantified before the test using a digital micrometer for 5 equally spaced positions along the measuring length. All dimensions were estimated using optimization routines minimizing fitting errors (e.g.: R and R' were fitted using circumference functions). Selected results are presented next.

3 EXPERIMENTAL RESULTS AND DISCUSSION

3.1 Mechanical Properties for the Studied Materials

Table 1 presents the main engineering mechanical properties obtained for the tested materials (Equation 1). Table 2, in its turn, presents obtained true properties including Bridgman's complete correction using image analysis results (Equations 2, 3 and 6). K and n were fitted between point Y and D illustrated by Figure 1c. As expected, it can be realized that a severe increase in true stress at fracture (σ_f) and true strain at fracture (ϵ_f) took place due to the use of corrected curves if compared to respective engineering data (S_f, e_f).

Table 1. Engineering mechanical properties for the materials considered for this study

Material	E (GPa)	S_{ys} (MPa)	S_{uts} (MPa)	S_f (MPa)	e_f (%)
AISI 1010	201.6 ± 3.3	280.0 ± 0.0	386.4 ± 2.8	261.9 ± 2.1	41.40 ± 0.01
AISI 1020	210.0 ± 3.4	205.7 ± 4.0	370.9 ± 0.8	274.1 ± 12.6	41.87 ± 0.02
AISI 4140	207.7 ± 1.4	385.0 ± 8.7	644.3 ± 20.9	515.1 ± 42.4	28.98 ± 0.04
ASTM A36	211.3 ± 8.2	286.7 ± 10.4	423.9 ± 16.2	239.7 ± 66.8	35.42 ± 0.01
ASTM A285	208.6 ± 1.7	209.3 ± 0.6	417.1 ± 3.1	287.5 ± 5.8	39.26 ± 2.10
ASTM A516	202.0 ± 0.2	286.5 ± 2.1	518.3 ± 3.8	384.3 ± 5.2	33.44 ± 1.50
AISI 304	154.6 ± 36.1	282.5 ± 10.6	631.6 ± 4.0	418.1 ± 19.7	75.61 ± 1.65
AISI 301	186.5 ± 2.6	453.3 ± 2.9	732.3 ± 10.2	498.8 ± 1.4	70.98 ± 1.80
SAF 2507	190.1 ± 2.4	631.0 ± 1.4	839.0 ± 7.2	554.8 ± 1.9	50.66 ± 0.06
Electrolytic Copper	72.9 ± 3.6	36.7 ± 5.0	211.1 ± 5.1	129.3 ± 13.6	59.29 ± 4.15

Table 2. True mechanical properties. σ_f and ε_f are obtained from the fracture point taking Bridgman's correction into account supported by real-time image analysis

Material	ε_{neck}	σ_f (MPa)	ε_f	K (MPa)	n
AISI 1010	0.2843	804.7 ± 79.6	1.0586 ± 0,0000	525.3	0.1149
AISI 1020	0.3233	704.6 ± 40.0	0.9244 ± 0.0004	560.2	0.1763
AISI 4140	0.2356	990.5 ± 37.7	0.6520 ± 0.0011	1010.3	0.1698
ASTM A36	0.2522	966.7 ± 31.2	1.1812 ± 0.0003	616.0	0.1414
ASTM A285	0.3084	674.1 ± 107.2	0.8433 ± 0.1718	701.9	0.2107
ASTM A516	0.2646	764.5 ± 53.1	0.6867 ± 0.0561	856.5	0.1924
AISI 304	0.5888	1874.5 ± 251.7	1.4450 ± 0.0148	1151.8	0.3028
AISI 301	0.4475	2017.2 ± 44.8	1.3973 ± 0.0251	1278.9	0.2523
SAF 2507	0.3089	1490.6 ± 4.9	0.9885 ± 0.0002	1207.0	0.1301
Electrolytic Copper	0.4015	498.4 ± 15.3	1.3487 ± 0.1229	494.8	0.4545

3.2 Necking Geometrical Evolution (Image Analysis)

Figure 4 illustrates necking evolution for ASTM A285 steel. Instantaneous strain (ε) and a/R levels are included for better comprehension. The first image represents the onset of necking while the last represents the onset of final fracture. All other materials presented essentially similar results and were not included due to space limitations. These frames are the basis for the developed image analysis technique.

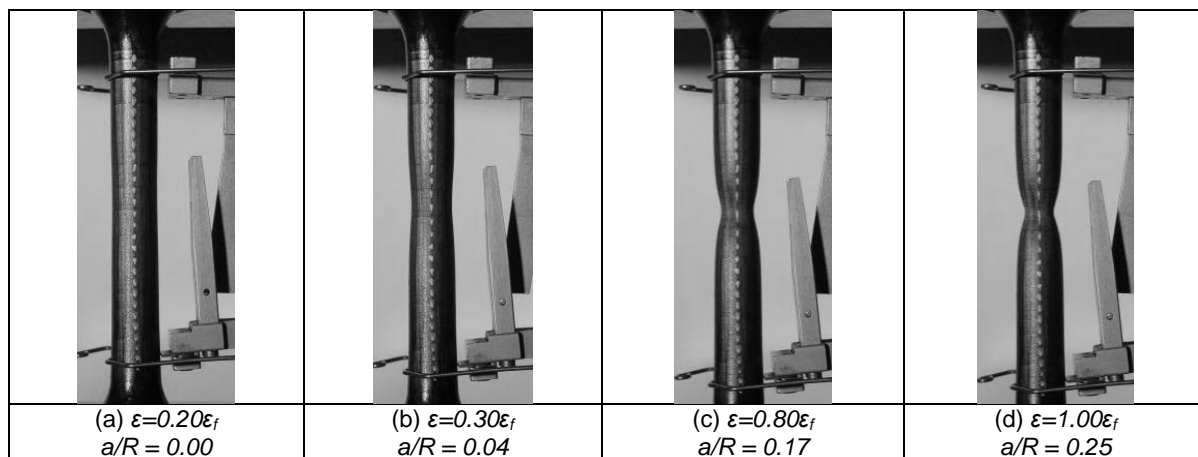


Figure 4. Neck evolution of a ASTM A285 steel specimen until fracture. Original diameter was 12.5 mm.

3.3 Proposed Dimensionless Parameters

Supported by the developed image analysis technique synchronized to load-displacement records from the MTS machine, the evolution of necking could be assessed for all tested materials as a function of true strain (ε). To overcome the effects of different hardening (Table 2) on strain levels for necking initiation,^(6,7) all results are presented as a function of ε_{tri} (Equation 9). Figures 5,6 present the main results for the accurate application of the proposed model (Equations 9 and 10). Figure 5 presents a/R vs. ε_{tri} evolutions for all materials. In most cases an excellent agreement was observed between different specimens for the same material and all materials presented a proportional (linear) relationship (a/R vs. ε_{tri}) until fracture (all fittings and correlation coefficients are included in the figures). These proportional evolutions are of great interest for validating the proposed (linear) refinements to Bridgman's model.

Comparing these results to Figure 3a – which includes results from Bridgman – some relevant conclusions emerge: i) the scatter using image analysis was remarkably lower; ii) achieved true strains are lower (maximum $\varepsilon_f \sim 1.445$ – Table 2), since Bridgman employed hydrostatic pressure in some tests to allow larger deformations; iii) for practical purposes, all tested materials could have its plastic instability until fracture represented by a linear regression model, different from Bridgman's proposals (Figure 3a); iv) with the smaller scatter found, one can conclude that each material presented a different neck geometrical evolution in terms of a/R vs. ε . Table 3 presents all calibrated ψ parameters from Figure 5 to be employed in the proposed model of Equation 10 and corroborate this fact. It is clear that deviations are quite small, even considering two or three valid specimens for each material, and that different materials presented different ψ values (even considering only steels or only stainless steels). Consequently, the simplified correction proposed by Bridgman (Equation 7) do not need (for practical purposes) to be described by a 3rd order polynomial and its applicability to all materials is not realistic.

One other detail that must be verified for the adequate application of equilibrium and displacements compatibility conditions is to which extent the osculating circle (of radius R – Figure 1) describes necking. The θ angle represents this validity circular sector. Theoretically, θ must be zero at the onset of necking and must increase during further straining configuring a “sharper” notch. The results from all image analyses were investigated and three conclusions emerged: i) the best fit for R using a circumference equation provided excellent agreement to real necking, thus necking of all materials can be precisely described by one single R value; ii) the same best fit provided θ values precisely connecting upper and lower inflection points of necking profile; iii) the evolution of θ vs. ε_{tri} was essentially proportional (linear) and initiating close to zero as expected based on solid mechanics. Figure 6 presents all results regarding θ vs. ε_{tri} evolution for all studied materials and conclusions are analogous to a/R results. Consequently, the validity of a single radius R in the description of necking is reasonable and θ values can be described as

$$\theta = \chi \varepsilon_{tri} = \chi (\varepsilon - \varepsilon_{neck}) \quad , \quad (11)$$

where χ is considered a material property, as assumed for ψ .

The agreement of neck geometry to the arc of a circle corroborated the work of Zhang and Li (which considered only Carbon steels).⁽¹³⁾ In addition, the model proposed by Equation 11 favors further investigations enforcing volume maintenance, equilibrium, compatibility and stress concentration of mild notches to enhance the accuracy of Bridgman's fields (Equation 5) for high strain levels (ε larger than ~ 0.60).

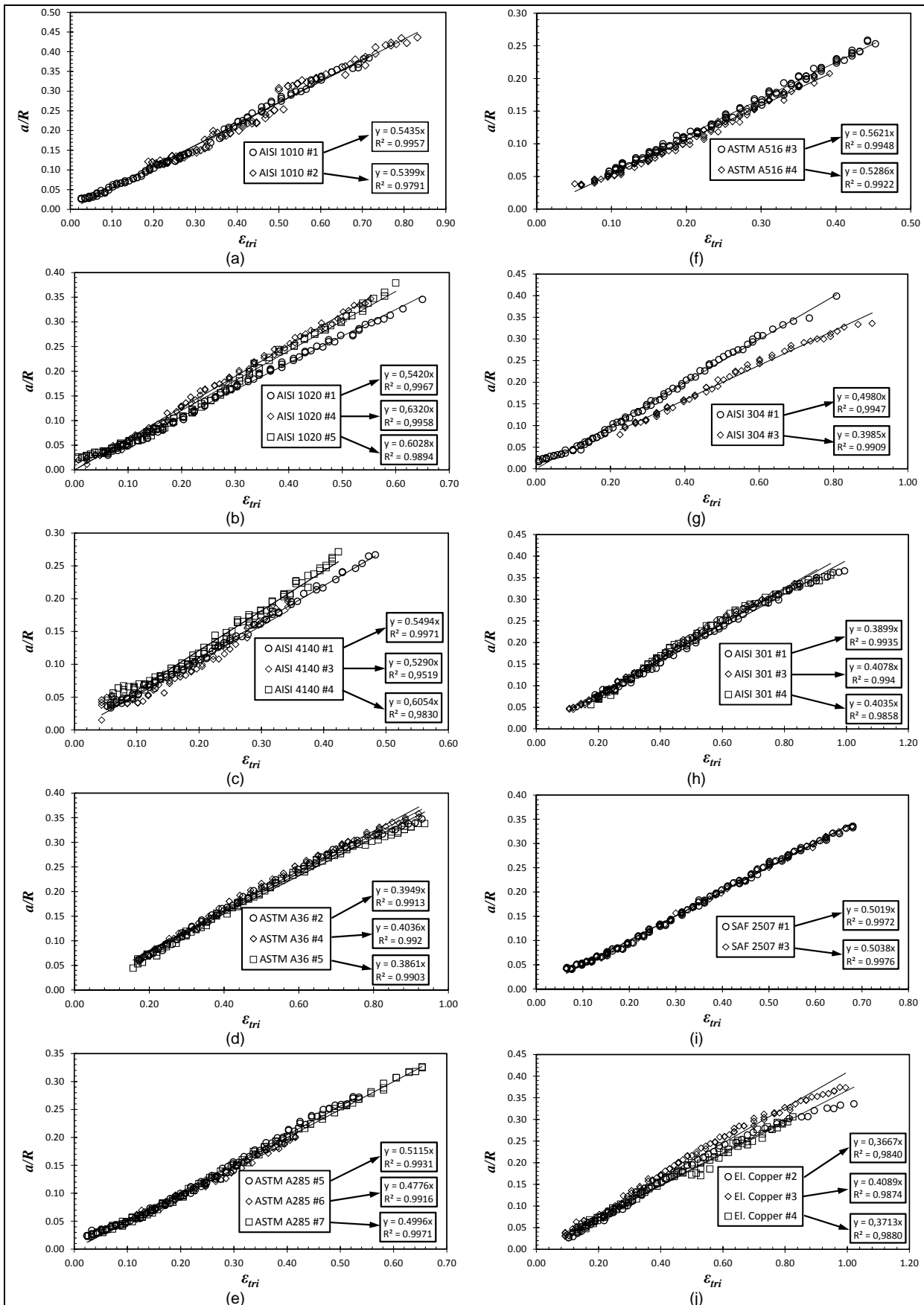


Figure 5. Neck geometry (a/R) as a function of ϵ_{iri} . (a) AISI 1010 carbon steel, (b) AISI 1020 carbon steel, (c) AISI 4140 alloy steel, (d) ASTMA36, (e) ASTMA285, (f) ASTMA516 Gr. 70 steel, (g) AISI304, (h) AISI 301, (i) SAF 2507 superduplex stainless steel and (j) electrolytic copper.

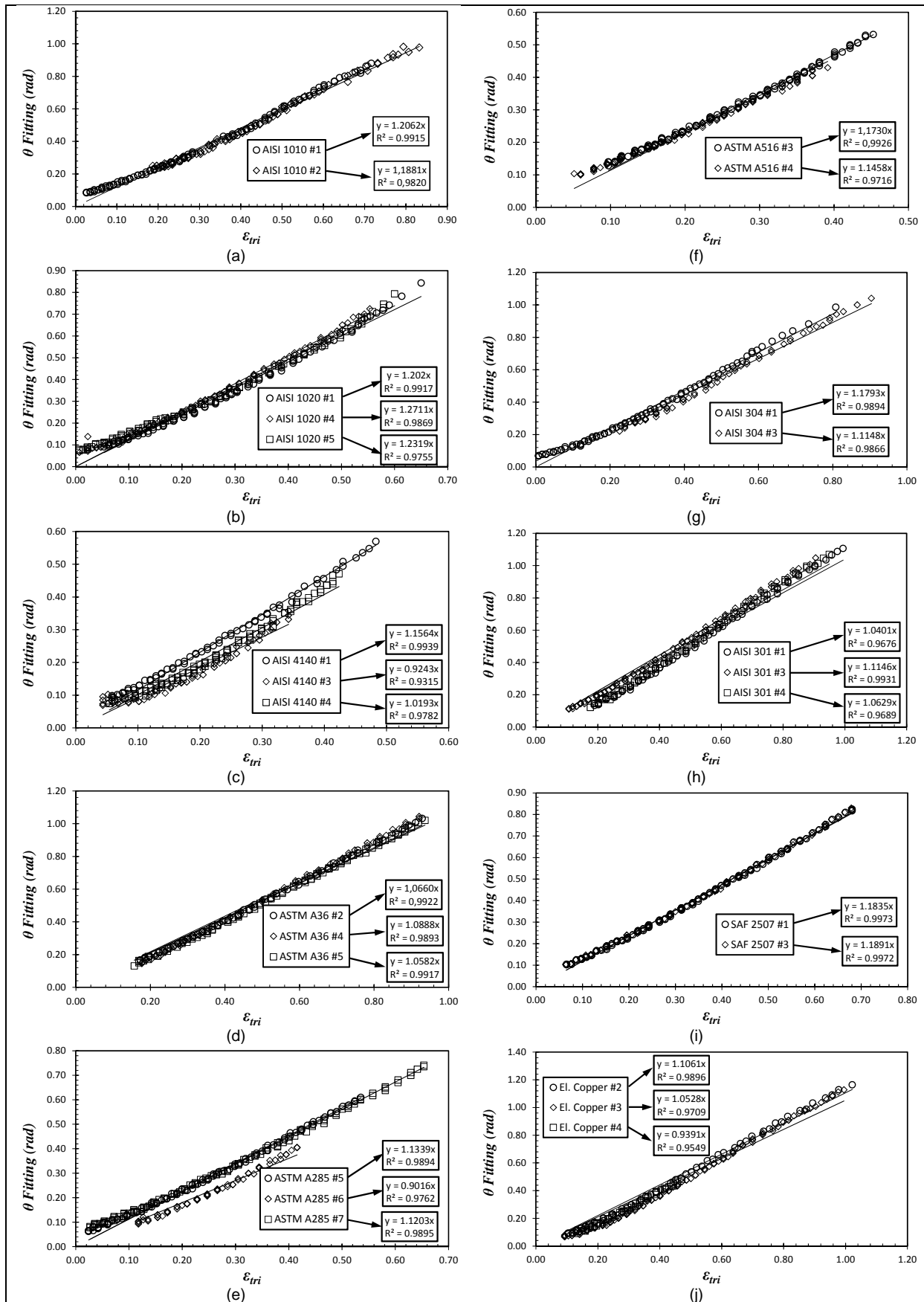


Figure 6. Neck fitting angle (θ) as a function of ϵ_{iri} . (a) AISI 1010 carbon steel, (b) AISI 1020 carbon steel, (c) AISI 4140 alloy steel, (d) ASTM A36, (e) ASTM A285, (f) ASTM A516 Gr. 70 steel, (g) AISI 304, (h) AISI 301, (i) SAF 2507 superduplex stainless steel and (j) electrolytic copper.

Table 3. Dimensionless parameters ψ and χ calibrated for all studied materials (Figures 5 and 6)

Material	ψ ()	χ ()
AISI 1010	0.5417 ± 0.0025	1.1972 ± 0.0128
AISI 1020	0.5923 ± 0.0459	1.2350 ± 0.0347
AISI 4140	0.5613 ± 0.0396	1.0333 ± 0.1167
ASTM A36	0.3949 ± 0.0088	1.0710 ± 0.0159
ASTM A285	0.4962 ± 0.0172	1.0519 ± 0.1304
ASTM A516	0.5454 ± 0.0237	1.1594 ± 0.0192
AISI 304	0.4483 ± 0.0704	1.1471 ± 0.0456
AISI 301	0.4004 ± 0.0093	1.0725 ± 0.0382
SAF 2507	0.5029 ± 0.0013	1.1863 ± 0.0040
Electrolytic Copper	0.3823 ± 0.0232	1.0327 ± 0.0853

For practical purposes, the main contribution of this work is the application of the proposed Equations (Equations 9 and 10) using ψ parameters to real tensile testing following a procedure which proved to be accurate and much simpler than full image analysis in the research group of current authors. The recommended practices follow:

- first, one tensile test should be conducted normally until final fracture.⁽¹⁶⁾ It provides the expected magnitude of ϵ_f and characterizes S - e plastic instability;
- a second tensile test should be conducted, but stopped for $\epsilon_{tri} \approx 0.8(\epsilon_f - \epsilon_{neck})$ using e_f and e_{neck} magnitudes (from first specimen) as a reference. The examination of this sample in a conventional profile projector provides “ a ” and the inflection points. R , θ and therefore ψ and χ for the material being studied derive from simple calculations (Equations 9 and 11);
- two additional samples should be tested and, after necking, paused when ϵ_{tri} reaches $\approx 20\%$, 40% , 60% , 80% and 90% of $(\epsilon_f - \epsilon_{neck})$. An automatic routine can be programmed using current servohydraulic testing machines. One must measure “ a ” in each pause with a simple digital paquimeter. Measurement of “ a ” from fractured specimen is also useful;
- the proposed model for triaxiality correction (Equation 10) can be directly applied providing σ - ϵ data until final fracture (at least 6 points between points D and F of Figure 1c). A σ - ϵ curve obtained using this protocol for SAF 2507 was provided to an FE model and the good agreement of Figure 3b emerged.

5 CONCLUDING REMARKS

This work investigates the geometrical evolution of necking on cylindrical conventional tensile specimens. The evolution of a/R and θ versus strain was investigated and a normalized strain quantity ($\epsilon_{tri} = \epsilon - \epsilon_{neck}$) was proposed. From the obtained results, an adapted Bridgman model could be proposed (Equation 10) to correct true stresses for triaxiality effects. Finally, a recommended practice was addressed in order to perform tensile testing with a minimum of simple physical measurements to provide accurate σ - ϵ data until final fracture. The following conclusions emerge:

- the scatter on measurements using high-definition images during necking is remarkably lower than those found in the literature, which suggests that the developed methodology is appropriate for further studies in the field;
- necking for all materials could be well described by an osculating circle (with radius R) combined to the minimum cross-section radius (a). In addition, the evolution of normalized neck geometry using these quantities (in the form a/R

and θ) provided for all tested materials proportional (linear) relationships (a/R vs. ε_{tri} and θ vs. ε_{tri}) until final fracture;

- two dimensionless parameters (ψ and χ) were proposed and, combined to the aforementioned linear evolutions fully describe necking geometry during deformation. They can be understood as material properties;
- however, different from Bridgman's conclusions based on Figure 3a, each material presented a different neck evolution in terms of geometry and strain level for the occurrence of instability (including different ψ and χ values). This makes Bridgman's simplified model (Equation 7) not realistic for practical applications;
- despite some simple measurements are still necessary, the proposed model of Equation 10 combined to the recommended practices for tensile testing is self-calibrated for each material being tested and provides accurate determination of true σ - ε properties until final fracture considering severe plasticity. Measurements during pauses were simple and didn't demand real-time onerous techniques.

Acknowledgment

This investigation was supported by FAPESP (Fundação de Amparo à Pesquisa do Estado de São Paulo), by the Brazilian Scientific Council for Research and Technology (CNPq - Grant 800277/2011-2) and by the Ignatian Educational Foundation (FEI, Brazil) through additional materials and human resources.

REFERENCES

- 1 GANHARUL, G. K. Q., AZEVEDO, N. B., DONATO, G. H. B., "Methods for the Experimental Evaluation of True Stress-Strain Curves After Necking of Conventional Tensile Specimens: Exploratory Investigation and Proposals"
- 2 ANDERSON, T. L., 2005, "Fracture Mechanics: Fundamentals and Applications" – 3rd edition, CRC Press, New York.
- 3 American Petroleum Institute, 2007, "Recommended Practice for Fitness-for-Service" – 2nd edition, API RP579-1.
- 4 B.S.I., 2005, "Guide on Methods for Assessing the Acceptability of Flaws in Metallic Structures", BS 7910.
- 5 DIETER, G. E., 1988, "Mechanical Metallurgy", 3rd edition, McGraw-Hill, UK.
- 6 RAGAB, A., BAYOUMI, S. E., 1998, "Eng. Solid Mechanics – Fundamentals and Applications, CRC Press, New York.
- 7 BRIDGMAN, P. W., 1952, "Studies in Large Plastic Flow and Fracture", MacGraw-Hill, New York.
- 8 DAVIDENKOV, N. N., SPIRIDONOVA, N. I., 1946, "Mechanical methods of testing analysis of the state of stress in the neck of a tension specimen", In: Proc. of ASTM, 46, p. 1147-1158.
- 9 LING, Y., 1996, "Uniaxial true stress-strain after necking", AMP Journal, 5, p. 38-48.
- 10 KAMAYA, M., KAWAKUBO, M., 2011, "A procedure for determining the true stress-strain curve over a large range of strains using digital image correlation and finite element analysis". Mech. of Materials, 43, p. 243-253.
- 11 JOUN, M., EOM, J. G., LEE, M. C., 2008, "A new method for acquiring true stress-strain curves over a large range of strains using a tensile test and finite element method". Mechanics of Materials, 40, p. 586-593.
- 12 THOMASON, P. F., 1969, "An analysis of necking in axisymmetric tension specimens", Int. Journal of Mechanical Science, 11, p. 481-490.

- 13 ZHANG, K. S., LI, Z. H., 1994, "Numerical analysis of the stress-strain curve and fracture initiation for ductile materials". Eng. Fracture Mechanics, 49, p. 235-241.
- 14 GANHARUL, G. K. Q., 2012, "Avaliação experimental e numérica do efeito da triaxialidade de tensões pós-instabilidade na determinação das propriedades tensão-deformação por meio do ensaio de tração uniaxial", master thesis, FEI University Center, Brasil.
- 15 AZEVEDO, N. B., DONATO, G. H. B., 2012, "Avaliação Numérico-Experimental da Evolução Geométrica da Estricção de Espécimes Cilíndricos de Tração", Proc. of II Symposium of Scientific Initiation of FEI University Center.
- 16 ASTM, 2009, "Standard Test Method for Tensile Testing of Metallic Materials", ASTM E8/E8M, Philadelphia.